Transition from leg to wing forces during take-off in birds

Pauline Provini[1, 2]; Bret W. Tobalske [3]; Kristen E. Crandell[3]; Anick Abourachid[1]

[1]Muséum National d'Histoire Naturelle, EGB, UMR 7179, 55 rue Buffon 75005 Paris, France

[2] Université Paris Descartes, 12 rue de l'Ecole de Médecine 75270 Paris, France

[3]Field Research Station at Fort Missoula, Division of Biological Sciences, University of Montana, Missoula, MT 59812, USA

Corresponding Author: P. Provini

Email: provini@mnhn.fr

Telephone: 33-1-40795714

Summary

Take-off mechanics are fundamental to the ecology and evolution of flying animals. Recent research reveals that initial take-off velocity in birds is driven mostly by hindlimbs forces. However, the contribution of the wings during the transition to air is unknown. To investigate this transition, we integrated measures of both leg and wing forces during take-off and the first three wingbeats in zebra finch (*Taeniopygia guttata*, 15g, N=7) and diamond dove (*Geopelia cuneata*, 50g, N=3). We measured ground-reaction forces produced by the hindlimbs using a perch mounted on a force-plate, whole body and wing kinematics using high-speed video, and aerodynamic forces using particle image velocimetry (PIV). Take-off performance was generally similar between species. When birds were perched, an acceleration peak produced by the legs contributed to 85±1% of the whole body resultant acceleration in finch and 77±6% in dove. At lift-off, coincident with the start of the first downstroke, the percentage of hindlimb contribution to initial flight velocity was 93.6±0.6%

in finch and 95.2±0.4% in dove. In finch, the first wingbeat produced 57.9±3.4% of the lift created during subsequent wingbeats compared to 62.5±2.2% in dove. Advance ratios were < 0.5 in both species, even when taking self-convection of shed vortices into account, so it was likely that wing-wake interactions dominated aerodynamics during wingbeats 2 and 3. These results underscore the relatively low contribution of the wings to initial take-off, and reveal a novel transitional role for the first wingbeat in terms of force production.

Key-words:

Zebra finch (*Taeniopygia guttata*)

Diamond dove (*Geopelia cuneata*)

Force

Take-off

Hindlimb

Forelimb

Velocity

Acceleration

Particle image velocimetry (PIV)

Introduction

Take-off initiates flight, and so plays a prominent role in the biology of flying birds. In living birds, take-off has an important function in predator-prey interactions, foraging, mate finding, and many other ecologically pertinent tasks. In addition, take-off was also a key component of the evolutionary origin of flight. Indeed, among the three main hypotheses proposed for the origin of flight in birds a transition between the substrate and the air is necessary before any possible kind of flight is accomplished, regardless of the substrate from which take-off takes place. These include the traditional "arboreal versus cursorial" origins, (Ostrom, 1974; Padian, 1987), and an alternative hypothesis involving wing assisted incline running (Dial, 2003). Thus, the debate about the origin of flight is closely linked to the ability to perform an effective take-off, and thus also to the contributions and coordination of the forelimbs and hindlimbs during this phase.

To date, only a small number of studies have focused on the mechanics of take-off in extant birds (Simpson, 1983; Heppner and Anderson, 1985; Dial and Biewener, 1993b; Bonser and Rayner, 1996; Tobalske et al., 2004; Berg and Biewener, 2010) and even fewer have done so in the context of the origin of avian flight (Gatesy and Dial, 1993; Earls, 2000; Dial et al., 2008). Furthermore, the majority of studies that have explored take-off in extant birds have either emphasized aerial performance and consequently focused on the use of wings during take-off (Norberg and Norberg, 1971; Simpson, 1983; Heppner and Anderson, 1985; Tobalske and Dial, 2000; Askew, 2001; Berg and Biewener, 2010) or have focused on the legs exclusively (Heppner and Anderson, 1985; Bonser and Rayner, 1996).

Only two studies have considered both locomotor systems during take-off (Earls, 2000; Tobalske et al., 2004). Kinematic and force plate analyses of birds with very different body shape and ecology (European starling (*Sturnus vulgaris*); Japanese quail (*Coturnix coturnix*) and rufous hummingbird (*Selasphorus rufus*), reveal that the hindlimbs rather than

the forelimbs are the primary accelerators during take-off. Because these prior studies have shown that the hindlimbs dominate, our effort in the present study is to compare in greater detail the relative contributions of legs and wings to take-off performance. Here, we directly measure the contribution to force production of both legs and wings to gain an understanding of the interaction between legs and wings in reference to timing and aerodynamic forces.

We chose two species for our investigation: zebra finch (*Taeniopygia guttata*) and diamond dove (*Geopelia cuneata*) because of their dissimilar wing shapes and upstroke kinematics. Zebra finches are passerine birds with rounded wings of low aspect ratio. They present a highly flexed posture during upstroke, commonly named a “feathered” upstroke (Tobalske et al., 1999; Tobalske et al., 2003). In contrast, diamond doves are columbids, have a pointed, high aspect-ratio wing, and use a “tip-reversal” upstroke during slow flight (Tobalske et al., 2003). We hypothesized this variation in wing kinematics may be crucial, as positioning the wings during the first upstroke appears to play a prominent role in the initial phase of take-off. Tip-reversal upstroke may enhance aerodynamic force production at this critical phase, even prior to the first downstroke. Indeed, it has been found that wings of birds using a tip-reversal upstroke (as pigeons, rock dove, *Columba livia*) are capable of producing substantial aerodynamic forces in the upstroke posture (Crandell and Tobalske, 2011). Moreover, pigeons can generate aerodynamic forces during tip-reversal upstroke in low speed turns (Ros et al., 2011).

We combined kinematic and dynamic analyses with particle image velocimetry (PIV) focusing on the first three wingbeats after lift-off. Previous analysis of starling and quail (Earls, 2000) measured take-off from a flat platform, which may heavily influence aerodynamic performance via complex interactions with the ground (Doligalski et al., 1994; Han and Cho, 2005). Thus our recordings were performed for a take-off from a perch. Our

novel exploration of aerodynamic performance will allow us to provide a more comprehensive understanding of the transition from terrestrial to aerial forces during take-off.

Materials and Methods

Animals

Seven zebra finch (*Taeniopygia guttata;* 15.4±1.8g, mean body mass (*m*) ± s.d.) and three diamond dove (*Geopelia cuneata*; 51.0±5.1g,) were purchased from commercial dealers, housed in flight cages, and provided with food and water *ad libitum*. Kinematics and force data collection were performed at the Muséum National d'Histoire Naturelle in Paris for three of the seven zebra finches. Kinematics, force and particle image velocimetry (PIV) data collection were performed at the Field Research Station in Missoula, Montana, USA, for four zebra finch and all three diamond dove. The animals were trained to take-off from a perch at a climb angle of ~45 degrees. All care and experimental procedures were approved by the University of Montana IACUC. We obtained morphometrics of these animals using standard techniques with the wings spread as in mid-downstroke (Tobalske et al., 2004) (Table 1). Herein, we report single wing length (cm), body width between the wings (cm), single wing projected surface area (cm^2), average wing chord (calculated as the width of the wing at one third away from shoulder**;** cm), aspect ratio (wing span divided by average wing chord, dimensionless) and tarsometatarsus length (cm).

Kinematics

In Paris, four digital high-speed video cameras (AVT Pike F-032B, Alliance Vision Technologies, Stadtroda, Germany) were positioned around the perch and take-offs were recorded at 200 Hz with a shutter speed of 300µs. The cameras were set in lateral, dorsal, oblique-frontal and frontal views and the overlapping fields of view of the cameras enabled a

three-dimensional reconstruction of the bird's movements during take-off, as well as during three complete wingbeat cycles after take-off. A checkerboard composed of 81 squares of 10mm×10mm was used to calibrate the cameras and scale the images. A MatLab (R2011b, Mathworks, Inc., Natick, MA, USA) custom M-file (Loco 3.3, Paul-Antoine Libourel MNHN) was used to extract the edge of the animal (head, tail and wings excluded) and calculate the coordinates of the centre of gravity from this shape (Fig. S1). The tip of the 9th primary of the left wing was digitized for the same trials. The digitization provided four sets of 2D coordinates for the centre of gravity and for the tip of the wing, used to calculate the 3D coordinates with a direct linear transform (DLT) routine (Hartley and Sturm, 1997). In Missoula, methods were similar, but we used four synchronized cameras, recording at 500 Hz and with a shutter speed of 143 µs. These included two Photron 1024 PCI (Photron, Inc., San Diego, CA, USA), one Photron SA-3, and one Phantom MiroEx4 (Vision Research Inc., Wayne, NJ, USA). The reconstruction of the centre of gravity of the shape formed by the edge of the bird was used as a proxy for the bird's centre of mass. A calculation of the actual centre of mass position using the multiple suspension method (Abourachid, 1993) for three zebra finches revealed that this centre of mass approximation was satisfactory: distance between the centre of gravity of the edge of the shape and the actual centre of mass: 6.4 mm ± 3.9, less than 7% of total length of the bird and less than 15% of maximal body width of the bird (Fig. S1). As birds flew within a vertical plane, approximately perpendicular to the perch, this point was used to calculate the two-dimensional trajectory of the animal (Fig. S2).

The trajectory of the animals was imposed by perch placement, set 0.75 m apart and inclined so that a line connecting the perches would be at 45 degrees above horizontal. Otherwise, the chosen flight path was not constrained, and variability of both the trajectory and body angle was relatively small. The mean magnitude of absolute deviations from the trajectory was 6.7±3.2 cm and varied from zero to 13.5±3.3 cm for zebra finch. In diamond

dove, the mean magnitude of absolute deviations from the trajectory was 5.4±3.6 cm and varied from zero to 10.9±3.8 cm. Body orientation was 16±5 degrees from horizontal for the zebra finch and 21±4 degrees for diamond dove (Fig. S2).

The component and resultant velocities ($m.s^{-1}$) and accelerations ($m.s^{-2}$) were calculated as the first and second derivatives of the trajectory, respectively. A MatLab (R2011b, The Mathworks, Inc., Natick, MA, USA) script allowed the reconstruction of the global orientation of the digitized shape, which was used to calculate the body angle (in degrees), corresponding to the angle between the body and the horizontal (Fig. S2).

The vertical trajectory of the tip of the 9th primary was used to define flight phases as it describes a succession of local maxima and minima that match upstroke/downstroke transition (USDS) and downstroke/upstroke transition (DSUS), respectively. The average of the wingbeat duration was calculated at different take-off phases. The beginning of the first upstroke was extracted (FW, "first use of the wings") as well as Lift-off (LO) corresponding to the last touch of the perch by the toes.

In our analysis, take-off was divided into four phases (Fig. 1E): 1) start take-off (t_0) when the bird is motionless on the perch, with folded wings and initiates countermovement, 2) wing and leg extension when the bird is still on the perch, 3) first downstroke and foot loses contact with perch (lift off, *LO*), 4) subsequent wingbeats with leg retraction against the body.

We calculated resultant acceleration using kinematic data ($\dot{V}_{RK}$), with gravitational acceleration (g, 9.8 m s^2) added to the vertical kinematic component ($\dot{V}_{ZK}$):

$$\dot{V}_{RK} = \sqrt{\dot{V}_{XK}^2 + \dot{V}_{YK}^2 + (\dot{V}_{ZK} + g)^2} \quad (1)$$

Where $\dot{V}_{XK}^2$= forward kinematic acceleration and $\dot{V}_{YK}^2$= lateral kinematic acceleration. We calculated average kinematic acceleration on the first upstroke duration (t_{up}, in ms). Average $\dot{V}_{RK}$ was compared to resultant acceleration calculated from the average ground

reaction force ($\dot{V}_{RFP}$, see below) during this period. Resultant acceleration calculated from the kinematics was also averaged on the duration of each wingbeat (t_{wb}, in ms) from the start of upstroke to the start of the next upstroke). This average $\dot{V}_{RK}$ was compared to resultant acceleration calculated using PIV data ($\dot{V}_{RPIV}$ see below).

Ground-reaction forces

In Paris, a wooden perch 1.5 cm in diameter and 8.5 cm long was mounted on a force platform (Kistler Squirrel force plate (Kistler France, Les Ulis, France, resolution ± 0.01N) with a top plate of 20cm×10cm and attached to a charge amplifier (Kistler type 9865). It was used to record the vertical and horizontal ground-reaction forces exerted on the perch at 400 Hz, using BioWare® Software Version 4.0.x Type 2812A (Kistler France).

The force perch in Montana was 1.3 cm in diameter, 7 cm long. It was covered in sandpaper to provide traction. The perch was mounted with its axis in line with the surface of a custom Bertec force plate (15 x 15 cm platform, 200 Hz resonant frequency, Bertec Corp., Columbus, OH, USA). Forces on the Bertec plate were digitally amplified 10x (Bertec AM6800) and recorded at 500 Hz using Chart software v4.5 (ADInstruments, Inc., Colorado Springs, CO, USA) and a Powerlab 8 SP A/D converter (ADInstruments Inc.).

Forces were filtered using a zero phase shift low-pass (50Hz) Butterworth filter. The resultant acceleration, measured using the force plate ($\dot{V}_{RFP}$) was calculated:

$$\dot{V}_{RFP} = \frac{\sqrt{F_x^2 + F_y^2 + F_z^2}}{m} \qquad (2)$$

Where F_x = forward force, F_y = lateral force, F_z = vertical force. For comparison with average $\dot{V}_{RK}$ during the first upstroke (i.e., during ground contact), we averaged $\dot{V}_{RFP}$ on t_{up}.

To measure the relative hindlimb contribution to initial resultant flight velocity (i.e., percent of V_{RK} comprised by V_{RFP}) at lift off (*LO*), we followed the methods of Earls (Earls, 2000) and integrated $\dot{V}_{RFP}$ with respect to time (t) from the beginning of take-off (t_0) to *LO*:

$$V_{RFP} = \int_{t_0}^{LO} \frac{\sqrt{F_X^2 + F_Y^2 + (F_Z - mg)^2}}{m} dt \quad (3)$$

Particle Image Velocimetry (PIV)

To compare aerodynamics with associated wingbeat kinematics, we used a synchronized high-speed video camera (Photron 1024 PCI (Photron USA Inc., San Diego, CA, USA)) sampling at 500 Hz, and located lateral to the animal. Data acquisition and analysis of PIV was performed using a LaVison GmBH (Goettingen, Germany) PIV system running DaVis 7.1 software. A dual-cavity pulsed 50-mJ Nd: YAG laser was used to illuminate a flow field of 3 mm thick, with planar dimensions spanning a field of 25×33 cm. The illumination field was cranial to the bird, parasagittal and mid-wing at the middle of downstroke (Spedding et al., 2003; Warrick et al., 2005). We seeded the air with particles of olive oil (<1 μm in diameter) generated at a rate of 7×10^{10} particles s^{-1} using a vaporizer fitted with a Laskin nozzle. Particle illumination was recorded using a 1376×1040 pixel, charged-coupled-device (CCD) camera placed perpendicular to the illumination field, and PIV samples were obtained at 5 Hz. To calculate particle velocity, we used cross-correlation of paired images with an elapsed time between images (Δt) of 500 μs. Average particle separation was 6 pixels in the centre of the animal's wake. We employed an adaptive multipass filter with an initial interrogation area of 64×64 pixels and final area of 16×16 pixels with 50% overlap. Vector fields were post processed using a median filter (strong removal if difference relative to average >3×r.m.s. of neighbours and iterative reinsertion if <3×r.m.s. of neighbours), removal of groups with <5 vectors, fill of all empty spaces by interpolation, and one pass of 3×3 smoothing. Subsequent analysis focused upon vortex cores.

We used streamlines, drawn with vectors expressed relative to average velocity, to inform our selection of regions of vorticity (ω, in s^{-1}), which is a measure of local change in velocity in the flow field (Spedding et al. 2003). We treated as background noise and masked from subsequent analysis $|\omega|<3$s.d. of $|\omega|$ in the free-stream. To measure circulation (Γ, $m^2 \cdot s^{-1}$) in vortex cores, we used methods adapted from Spedding et al. (Spedding et al., 2003). We integrated all same-sign ω in a given PIV field within 1.5 chord lengths of peak ω to measure Γ (e.g., Fig. 3). We considered each negatively-signed vortex core deposited in the wake during early downstroke to represent the cross section of a starting vortex shed from the trailing edge of the wing, equal in magnitude but opposite in sign from the bound vortex on the wing as lift development began during downstroke. Similarly, we considered each positively signed vortex core deposited in the wake during late downstroke to represent the cross-section of an ending vortex shed from the trailing edge of the wing.

We estimated average lift during the entire wingbeat (*L*) by coupling our PIV data with separately acquired three-dimensional kinematic data for the same test subjects ((Spedding et al., 2003; Warrick et al., 2005; Tobalske and Dial, 2007) see *Kinematics*, above). Note that *L* includes vertical (weight support) and horizontal (thrust) components. Average *L* was estimated:

$$L = \rho \frac{A(\Gamma + cSV_{vort})}{t_{wb}} \qquad (4)$$

where ρ is air density (air density in Missoula at 1000 m in altitude is 1.06±0.01kg.m^{-3}), *A* is the area swept by the two wings during each downstroke, not including the body, c is added-mass coefficient (Dabiri, 2005), *S* is average diameter of observed vortex cores, and V_{vort} is self-induced vortex velocity (Dabiri, 2005). Following Spedding et al. (Spedding et al., 2003) and Warrick et al. (Warrick et al., 2005), we assumed that a single vortex loop shed per downstroke and that no contraction occurred during wake development. We assumed c=0.72 as the added-mass coefficient previously reported for an elliptical vortex (Dabiri, 2005). We

measured V_{vort} as observed rate of translation of ω_{max} in the subset (N=37 for zebra finch and N=42 for diamond dove) of our PIV samples in which the same vortex core appeared in consecutive images. We also measured the magnitude and angle from horizontal for induced velocity (m s^{-1}) in the middle of the shed vortices (Tobalske and Dial, 2007).

We estimated average acceleration using the PIV data ($\dot{V}_{RPIV}$), which was the acceleration due to aerodynamic force produced during each wingbeat:

$$\dot{V}_{RPIV} = \frac{L}{m} \quad (5)$$

Advance ratio

To provide insight into the potential for wing-wake interaction and other unsteady aerodynamic effects (Spedding, 1993; Dickinson et al., 1999) to dominate wing function during take-off, we calculated advance ratio (dimensionless) using kinematic data (J_K) and using kinematics coupled with PIV data (J_{PIV}). Advance ratio in aeronautical engineering is an expression of aircraft velocity divided by the tip velocity of the aircraft's propeller, or, equivalently, distance travelled by the aircraft relative to the excursion of the propeller tip during one revolution (Vogel, 1994). Rather than assume sinusoidal motion of the oscillating wing as is traditionally done when adapting propeller equations to model advance ratio in animals that oscillate their wings (Ellington, 1984; Vogel, 1994), we used observed three-dimensional wingtip velocity relative to the bird (V_{wtip}). Thus:

$$J_K = \frac{V_{RK}}{V_{wtip}} \quad (6)$$

and

$$J_{PIV} = \frac{D_{wake}}{t_{wb} V_{wtip}} \quad (7)$$

Where D_{wake} = the average distance (m) between vortices in the wake. Note that Eq. (7) includes the contribution of self-convection of shed vortices:

$$\frac{D_{wake}}{t_{wb}} \cong V_{RK} + V_{vort} \quad (8)$$

J_{PIV} was undefined for wingbeat one, as it lacks a previously shed vortex (D_{wake} was undefined).

Statistics

To test for differences in the timing of first downstroke and *LO*, we used two-way repeated measures ANOVA with time and individual as factors and taking into account the trial repetition and species.

We also used two-way repeated measures ANOVA to test for a statistically-significant difference between wingbeat 1 and subsequent wingbeats for *L*, angle magnitude of induced velocity in the wake and J_K. Wingbeat and individuals were used as factor and the trial repetition was also taken into account for both species.

Lastly, t-tests were used to compare data sets coming from kinematic analysis with data sets coming from ground reaction force or aerodynamic analyses. All statistical tests were performed using R (Package *stats* version 2.15.0 (R Development Core Team, 2010)). Throughout, we report mean ± s.d..

Results

Kinematics

During the preparation to take-off each bird crouched from a standing position. This counter movement (starting at time t_0) was visible in both species but was more evident in diamond dove, with a lower body angle before *LO* (16.3±5.3 degrees) compared with the zebra finch (20.1±7.3 degrees) (Fig. S2). During the second phase of take-off, the birds start extending their hindlimbs and forelimbs. This happened at 28.3±7.6 ms before *LO* in zebra finch compared to 38.9±8.10ms before *LO* in diamond dove. This is about 80% and 60% of the time from the start of counter movement (t_0) to *LO* in the zebra finch and diamond dove,

respectively. Both species started their first downstroke after their feet were completely off the perch (2 ms delay in the zebra finch, 6 ms in the diamond dove). However, these differences in timing were not statistically significant (zebra finch: ANOVA: factor=timing: $F_{1,26}$=0.01; P>0.9; factor=individuals: $F_{1,3}$=0.02; P>0.7; in diamond dove: ANOVA: factor=timing: $F_{1,9}$=4.9; P>0.06; factor=individuals: $F_{1,2}$=0.04; P>0.2) and, it should be noted that 2 ms was the margin of error for our video sampling at 500 Hz. The first wingbeat ends 24.5±6.1ms after lift-off in zebra finch compared to 37.9±6.2 ms in diamond dove. In zebra finch, each wingbeat lasts approximately 50ms, compared to 70ms in diamond dove. These durations are nearly equivalent in terms of the total wingbeat cycle, at 52.3% in the zebra finch and 54.1% in the diamond dove.

In both species, V_{RK} increased during the first two phases of take-off (Fig. 1A, C). In zebra finch the V_{RK} increased from 0.03±0.03m.s^{-1} at t_0 to 1.74±0.3m.s^{-1} at *LO*. In diamond dove, the V_{RK} increased from 0.04±0.1m.s^{-1} to 1.29±0.1m.s^{-1} at *LO*. After *LO*, V_{RK} remained fairly constant during the first three wingbeats and reached 1.8±0.6m.s^{-1} in zebra finch and 1.7±0.1m.s^{-1} in diamond dove. The V_{RK} at *LO* corresponded to 92.3±4.2% of the maximal V_{RK} reached during the first wingbeat in zebra finch and 79.4±3.9% in diamond dove.

The acceleration profile shows a peak during the perching phase of take-off. In zebra finch, $\dot{V}_{RK}$ reached 47.2±14.4 m.s^{-2} (4.8 × body weight), and occurred 28.3±6.0 ms before *LO* (Fig. 1B). In diamond dove, $\dot{V}_{RK}$ reached 26.7±3.2m.s^{-2} (2.7 × body weight) and occurred 23.5±7.9 ms before LO (Fig. 1D). These times are 80.6 % and 76.5% of the interval between t_0 and *LO* in zebra finch and diamond dove, respectively.

Force production of legs

The $\dot{V}_{RFP}$ produced during take-off, calculated using ground-reaction force, was 47.8±7.5 m.s^{-2} in zebra finch, compared to 26.7±7.0 m.s^{-2} in diamond dove (Fig.2A, C). Thus,

the maximal leg force produced by the animal corresponds to 4.9±0.7 × body weight for zebra finch and 2.7±0.3 × body weight for diamond dove. Average $\dot{V}_{RFP}$ during the first upstroke was 35.5±18.0 m.s^{-2} in zebra finch and 25.2±8.8 m.s^{-2} in diamond dove (Fig. 4). The peak V_{RFP} was 1.78±0.6 m.s^{-1} at LO in zebra finch and 1.2±0.4 m.s^{-1} in diamond dove (Fig. 2 B, D).

Force production of the wings.

For zebra finch, the first wingbeat produced significantly less *L* than the second and third ones (ANOVA: factor = wingbeat: $F_{1, 27}$=16.03; P < 0.001; factor=individuals: $F_{1, 3}$= 0.9; P > 0.1). Therefore, for the first wingbeat, *L* represented 0.9±0.4 × body weight, whereas it comprised 1.4±0.6 × body weight for the second wingbeat and 1.7±0.2 for the third one. The $\dot{V}_{RPIV}$ produced during the first wingbeat was 58±3.4% of that during the second and third wingbeats (Fig. 4A). Considering the relevant variables for estimating *L* (Eq. 4; Table 2A) the differences were due to less circulation (Γ), a smaller area (*A*) of the vortex loop and a lower induced velocity during the first wingbeat, compared to the subsequent wingbeats. Angle of the induced velocity in the wake for all three wingbeats was not significantly different among wingbeats (ANOVA: factor = wingbeat: $F_{1, 18}$= 0.11; P > 0.7; factor=individuals: $F_{3, 18}$= 2.3; P < 0.1). Although the general trend was for induced velocity to increase with wingbeat number, high variability meant that induced velocity of the first wingbeat, 3.9±1.8 m s^{-1}, was not significantly less than the second (5.1±2.3m s^{-1}) and third wingbeat (5.1±1.6 m s^{-1}).

For diamond dove, the first wingbeat also produced significantly less *L* than the subsequent ones (ANOVA: factor = wingbeat: $F_{1, 35}$=5.6; P < 0.05; factor=individuals: $F_{1, 2}$= 1.6; P>0.2). For the first wingbeat, *L* was 0.9±0.3 × body weight, 1.1±0.0.3 for the second wingbeat, and 1.7±0.6 for the third wingbeat. The first wingbeat comprised 63±5.2% of $\dot{V}_{RPIV}$produced during the subsequent wingbeats (Fig. 4B). As in the finch, less *L* was associated with less Γ and a lower induced velocity in wingbeat 1 (Table 2B). Angle of the

induced velocity for the first wingbeat was significantly lower than the second (ANOVA: factor = wingbeat: $F_{1, 23}$= 43.5; P< 0.001; factor=individuals: $F_{2, 23}$= 1.8; P > 0.1). Induced velocity for the first wingbeat was 4.4±1.3m s^{-1}, and 5.2±1.1m s^{-1} for the second wingbeat. These values were statistically different (ANOVA: factor = wingbeat: $F_{1, 32}$= 8.7; P < 0. 006; factor = individual: $F_{2, 32}$= 2.8; P > 0. 07).

Comparison of wing and leg contributions

During the first phase of take-off, when the bird was on the perch with folded wings, V_{RFP} was similar to V_R in both species (for zebra finch: T-test: df = 13, P > 0. 7; for diamond dove: T-test: df = 12, P > 0.5) (Fig 2B, D). Both $\dot{V}_{RFP}$ *and* $\dot{V}_{RR}$ followed a similar pattern in both species (for zebra finch: t-test: df = 13, P > 0. 6; for diamond dove: t-test: df = 12, P > 0.21) (Fig. 2A, C). This means that during the first phase of take-off the legs are responsible for the entire resultant velocity and resultant acceleration.

During the second phase of take-off, when the wings were unfolded, $\dot{V}_{RFP}$ was lower than $\dot{V}_{RR}$, 34.56±7.9 m.s^{-2} for $\dot{V}_{RFP}$ compared to 43.63±6.45 m.s^{-2} for $\dot{V}_{RR}$ in zebra finch, and 24.51±3.18 m.s^{-2} for the $\dot{V}_{RFP}$ compared to 33.21±1.8 m.s^{-2} for $\dot{V}_{RR}$ in diamond dove (Fig. 4A, B). Moreover, at LO, V_{RFP} was 93.6±0.6% of the V_{RR} in zebra finch, and 95.2±0.4% of V_{RR} in diamond dove (Fig 2B, D). Average $\dot{V}_{RFP}$ during the second phase of take-off was significantly different from $\dot{V}_{RR}$ (for zebra finch: t-test: df = 13, P < 0.05; for diamond dove: t-test: df = 12, P < 0.05).

After *LO*, the $\dot{V}_{RR}$ during the first wingbeat was significantly different from $\dot{V}_{RP\,IV}$ (for zebra finch: t-test: df = 13, P < 0.001; for diamond dove: t-test: df = 12, P < 0.001). But we can notice that for wingbeat 1, $\dot{V}_{RR}$ is approximately equal to the sum of $\dot{V}_{RFP}$ and $\dot{V}_{RP\,IV}$.

During the following wingbeats (Fig.4) there was no significant difference in the $\dot{V}_{RPIV}$ compared with $\dot{V}_{RK}$ (for the second wingbeat in zebra finch: t-test: df = 13, P = 0.37; for diamond dove: t-test: df = 12, P = 0.20).

Advance ratio measured using kinematics (J_K) did not differ significantly between wingbeats (for zebra finch: ANOVA: factor = wingbeat: $F_{2,3}$= 3.0; P > 0.1; factor=individuals: $F_{1,3}$= 0.14; P > 0.7; for diamond dove: ANOVA: factor = wingbeat: $F_{2,3}$= 0.65; P > 0.5; factor=individuals : $F_{1,3}$= 0.03; P > 0.8), or among species (ANOVA: factor = species: $F_{1,14}$= 3.31; P > 0.09; factor=individuals : $F_{1,14}$= 0.14; P > 0.7).

But J_{PIV} was significantly larger in zebra finch (~ 0.40) compared with diamond dove (~0.30) during wingbeats 2 and 3 (t-test: df = 5, P < 0.0003), and J_{PIV} was always greater than J_K (t-test: df = 11, P < 0.0001) which varied from 0.17 – 0.32 (Table 2).

Discussion

The wings of birds have historically been considered as the primary force producers during take-off (Rüppell, 1975; Heppner and Anderson, 1985). However, more recent studies (Earls, 2000; Tobalske, 2004; Berg and Biewener, 2010) agree that the legs play a key role in producing the acceleration needed for take-off. By combining three different data sets to calculate force production we were able to assess the relative role of both hindlimbs and forelimbs through take-off in two new species of birds with different wing shape and ecology. Our data show that in zebra finch, a small passerine, and in diamond dove, a small columbid, the hindlimbs and forelimbs are successively used, with hindlimb dominance in the first phases of take-off providing initial acceleration, and coordinated use of wings to maintain velocity through the first three wingbeats. Despite dramatic differences in body size, wing morphology (Table 1) and slow-flight kinematics (Tobalske, 2007), we did not observe significant differences between species in aerodynamic force produced. Rather, the most

prominent difference between birds was observed at the initial acceleration - due almost exclusively to the hindlimbs - and subsequent flight velocity upon leaving the perch, both of which were greater in the zebra finch versus the dove.

During the first phase of take-off, the resultant acceleration calculated from the force data ($\dot{V}_{RFP}$) was not significantly different from the resultant acceleration calculated from the kinematic data ($\dot{V}_{RK}$, Figs 1 and 2), indicating that legs were wholly responsible for the acceleration while on contact with the perch during preparation to take-off. An acceleration peak is observed in both species, with a magnitude four times greater than that observed after lift-off (*LO*). We can notice that this acceleration peak occurred at the transition between the first and the second phase of take-off in zebra finch (28.3±6.0 ms before lift-off) whereas it happened slightly after the beginning of the first upstroke in diamond dove (15.35±4.2ms after the beginning of the second phase) (Fig. 1B and D). For both birds, this acceleration peak occurs while still on the perch. The observed maximal vertical force production (F_z) was greater than what is reported in other studies: from 1.3–2.3 × body weight in the pigeon compared to 2.9-3.6 in diamond dove and 3.6-8.3 in zebra finch (Clark and Alexander, 1975; Heppner and Anderson, 1985; Bonser and Rayner, 1996). We also observed that relative hindlimb forces produced by the dove (50 g) were 55±2.5% lower than the finch (15 g), which was consistent with the hypothesis that the maximal acceleration generated across species should be inversely proportional to body weight (Bonser and Rayner, 1996).

In the second phase of take-off, corresponding to the first upstroke, the average $\dot{V}_{RFP}$ represented 93±0.6% of the resultant acceleration calculated from the kinematic data for zebra finch and 92.1±0.4% for diamond dove (Fig. 4). This indicates a combined action of the hindlimbs with the forelimbs, although the hindlimbs dominated. The wings started to unfold at the same moment as the acceleration profiles of ground reaction forces and kinematics start

to diverge (Fig. 2A, C). We can suggest that forces produced by the wings (Crandell and Tobalske, 2011; Ros et al., 2011) may be responsible for a part of the observed disparity between ground reaction forces and observed kinematics in diamond dove. However, it seems unlikely that zebra finch is generating an aerodynamically-active upstroke, as the species uses a flexed-wing upstroke (Tobalske et al., 1999), and no aerodynamic activity was visible in the wake. The bird's body is rotating upward as legs are extending and this rotational kinematics acceleration might be added inappropriately to our linear $\dot{V}_{RK}$, thus leading to an overestimation of its magnitude. In any case, our data show that in both species, the initial acceleration peak is predominantly due to the hindlimbs, with the legs contributing to approximately 70-80% of $\dot{V}_{RK}$ produced during the second phase of take-off.

Surprisingly, despite large differences in leg and wing morphology (Table 1), both species appear to promote similar tactics of wing and leg use. However, in comparing maximal velocity of the first wingbeat (V_{RK}) to that produced by the legs (V_{FP}) *at LO*, an interesting pattern emerges. In zebra finch, 92.3±4.2% of the maximal velocity was reached by *LO*, and only 79.36±3.9% in diamond dove (Fig 2B, D). Observed velocities produced by the leg forces were on the high end of the range that has previously been reported for European starling, Japanese quail, rufous hummingbird, and pigeon; for which the percentage of velocity reached at *LO* corresponds to between 59% and 90% of the velocity achieved at the next upstroke/downstroke transition (Earls, 2000; Tobalske, 2004; Berg and Biewener, 2010). In comparing magnitude of resultant acceleration previously reported with data from the present study, we see that both the zebra finch (4.4m.s^{-2}) and diamond dove (3.4m.s^{-2}) were near the European starling (4.3m.s^{-2}) (Earls, 2000). All three of these species are ecological generalists in their respective habitats, and legs contribute to 92%, 79%, and 95% of total velocity respectively by take-off. In contrast, the resultant acceleration of a highly specialized aerial bird, the rufous hummingbird, is 1.78m.s^{-2} with legs contributing to only

60% of total velocity (Tobalske et al., 2004). On the other end of the spectrum, the Japanese quail, a ground specialist, produces an acceleration maximum of 8.3m.s^{-2}, contributing to 89% body velocity. This continuum suggests the interaction between wings and legs should be framed in an ecological context, and merits further exploration with a larger sample size.

In both zebra finch and diamond dove, the beginning of the first downstroke occurs approximately a few milliseconds after the bird leaves the perch, resulting in a discrete succession in the use of the hindlimbs and forelimbs. However, we can concede that the relative timing of the different phases of take-off is closely related to the animal's state of stress. Informally, we observed that the more the bird was stressed, the earlier the wings would start to be used which is consistent with the previous studies on take-off (Earls, 2000; Tobalske et al., 2004). In this study, only trials with spontaneous, unstressed take-off were analyzed, resulting in a low variability in the timing of take-off phases.

In the aerial phase of take-off, our data show that during the first wingbeat, the acceleration calculated from the PIV data ($\dot{V}_{RPIV}$) represented only 24.8±4.2% of $\dot{V}_{RM}$ in zebra finch and 29.9±3.6% in diamond dove. This further demonstrates that during the first wingbeat, the resultant acceleration is mostly due to the hindlimb contribution, with wings contributing to about 30% of this acceleration. Moreover, we can note that lift production (L) during the first wingbeat represents only 58±3.4% of the force produced by the subsequent wingbeats in zebra finch and 63±5.2 in diamond dove. Both finch and dove did not produce enough force in the first wingbeat to support bodyweight in the air (0.9 ± 0.4 and 0.9 ± 0.3 × bodyweight respectively), but, given the large standard deviations (Fig. 4), they may have supported body weight some of the time. Regardless, this minimal force production was not enough to accelerate quickly without relying on the initial acceleration of the legs. This is compensated by the following wingbeats, where force production increased well above that required for support of body weight (1.4 and 1.7 for finch and 1.1 and 1.7 for dove),

indicating force used toward net acceleration. Relatively large standard deviations for L and $\dot{V}_{RPIV}$ may also be linked to motivational differences between trials.

Both bird species follow a general pattern in force production by the wings, producing near minimal required to counter gravity and then increasing with subsequent wingbeats. This implies that generalist birds may have tuned the timing and magnitude of force production by the wings to accommodate neuromuscular, aerodynamic or environmental constraints. Our estimates of lift that increase with each wingbeat during take-off are consistent with direct measures of muscle activity in pigeons in which the pectoralis muscles are recruited at lower levels and produce lower force during the first wingbeat compared with subsequent wingbeats (Dial and Biewener, 1993a; Tobalske and Biewener, 2008). Several mechanisms may explain this variation in force production. One hypothesis we suggest is the birds may capitalize on a mechanism similar to wake-recapture (Sane, 2003) the subsequent wingbeats are capable of capitalizing on induced flow from previous wingbeats. If this is the case, the first wingbeat is incapable of benefiting from induced flow, and may, therefore, exhibit weaker lift. Our observed low advance ratios (J_K and J_{PIV}; Table 2) suggest that wings may interact with previously shed circulation in the wake (Spedding, 1993). Even accounting for the contribution of self-convection of shed vortices away from the flying animal (V_{vort}), advance ratios were considerably less than 1 (J_{PIV}, Table 2). This revealed that the wingtips were always moving much further than the body during a given wingbeat. Another possible influence is the orientation of the body relative to the wake changes from first to subsequent wingbeats (Table 2; S2), and body angle may initially be in an unfavorable orientation. In this case, angle of induced downwash in the finch was not statistically different from the first to subsequent wingbeats, but diamond dove angle of induced velocity was different, suggesting doves may be under pressure to reorient their body, but not finches. Finally, there may be a need to provide enough space for the wings to complete a full downstroke without hitting the

substratum and risking wing damage (Heppner and Anderson, 1985). Thus, the wings are spatially limited and complete a smaller arc. Clearly, further studies of potential unsteady aerodynamic performance and the interactions between substrate and air are necessary.

In the zebra finch, the acceleration produced by the wings during the first wingbeat ($\dot{V}_{RH}$ and $\dot{V}_{PIV}$) represents a lower proportion of the acceleration produced during the subsequent wingbeats than in diamond dove (Figs. 2 and 4). Diamond doves use a tip-reversal upstroke, and we hypothesize that this style of upstroke is aerodynamically active (Crandell and Tobalske, 2011; Ros et al., 2011). Tip-reversal may provide an earlier onset of useful aerodynamic force production during the first wingbeat in diamond dove. Due to the interaction of body mass with acceleration in the present study, this suggestion must be interpreted as tentative. It would be useful to test this hypothesis within a clade that exhibits variation in body mass and upstroke style.

During take-off, the amount of acceleration produced by the hindlimbs is much higher than the acceleration produced by the forelimbs. It can be linked to the fact that it is more efficient to push against the ground than against the air (Dickinson et al., 2000). These data emphasize the prominent role of the hindlimbs in all avian locomotor behaviors except flight (Dial, 2003; Abourachid et al., 2011; Provini et al., 2012). This work suggests that during the transitional first wingbeat timing coordination exists between wings and legs, which can be seen as anatomical and neuromuscular systems, previously identified as “modules” in birds (Gatesy and Dial, 1996). Our results combined with previous work (Earls, 2000; Tobalske et al., 2004) support the general conclusion underscoring the prominent role of hindlimbs during take-off in a phylogenetically, morphologically and ecologically diverse array of birds. More extensive phylogenetic analysis is warranted to test the generality of the hypothesis of a universal hindlimb drive during take-off in birds. But, if this pattern is universal, this would provide support for the leaping model for the origin of flight (Garner et al., 1999). Indeed, in

cursorial theropod dinosaurs, powerful hindlimbs would have been a useful preadaptation to a hindlimb driven take-off. Moreover, in our study, we see incremental use of the flight apparatus for the first wingbeat, as suggested by the work of Jackson et al. (Jackson and Dial, 2011) on WAIR (wing-assisted incline running) where birds use rapid flapping of the wings to run up inclined surfaces. Even though we studied a standing take-off instead of WAIR, our data suggest that incremental use of the pectoralis muscle can modulate leg performance and contribute to weight support, and thus is a relevant model for the evolutionary origin of flapping. Therefore, our results may provide novel insights on the origin of avian flight as they are consistent with both leaping and WAIR models (Garner et al., 1999; Dial, 2003) with a hindlimb driven take-off assisted by a gradual use of the forelimb through the first wingbeats.

List of symbols

PIV	particle image velocimetry
USDS	upstroke/downstroke transition
DSUS	downstroke/upstroke transition
FW	First use of the wings
LO	Lift-off
c	vortex added mass coefficient
g	gravitational acceleration
m	body mass
t	time
t_0	start of take-off with countermovement
t_{up}	1st upstroke duration
t_{wb}	full wingbeat duration
A	loop area of wake vortex
D_{wake}	distance between shed vortices
F_X	forward force
F_Y	lateral force
F_Z	vertical force
J_k	advance ratio from kinematics
J_{PIV}	advance ratio from kinematics and aerodynamics
L	average lift
S	width of wake vortex
V_{RFP}	velocity calculated using data from force plate

V_{RK}	velocity calculated using kinematic data
V_{vort}	Self-convection velocity of shed vortices
$\dot{V}_{RFP}$	Acceleration calculated using data from force plate
$\dot{V}_{RK}$	Acceleration calculated using kinematics
$\dot{V}_{RPIV}$	Average acceleration calculated from PIV and kinematics
$\dot{V}_{XK}$	Forward acceleration calculated from kinematics
$\dot{V}_{YK}$	Lateral acceleration calculated from kinematics
$\dot{V}_{ZK}$	Vertical acceleration calculated from kinematics
Δt	elapsed time between PIV paired images
ω	vorticity
Γ	circulation
ρ	air density

Acknowledgments

We are grateful to Paul-Antoine Libourel, Hugues Clamouze and Brandon Jackson for their help during the experiments. Thanks to Bieke Van Hooydonck and Anthony Herrel for the force platform used in Paris. Thanks to Camille Dégardin for her help with the illustrations. This research was supported by grants from the UMR 7179, ATM Formes (MNHN) and from ED-FdV and Bettencourt-Schueller foundation fellowships as well as NSF grants IOS-0923606 and IOS-0919799.

References

Abourachid, A. (1993). Mechanics of standing in birds - Functional explanation of lameless problems in giant turkeys. *British Poultry Science* **34**, 887-898.

Abourachid, A., Hackert, R., Herbin, M., Libourel, P. A., Lambert, F., Gioanni, H., Provini, P., Blazevic, P. and Hugel, V. (2011). Bird terrestrial locomotion as revealed by 3D kinematics. *Zoology* **114**, 360– 368.

Askew, G. N., Marsh, R. L., Ellington, C. P. (2001). The mechanical power output of the flight muscles of blue-breasted quail (*Coturnix chinensis*) during take-off. *Journal of Experimental Biology* **204**, 3601-3619.

589 **Berg, A. M. and Biewener, A. A.** (2010). Wing and body kinematics of takeoff and landing
590 flight in the pigeon (*Columba livia*). *Journal of Experimental Biology* **213**, 1651-1658.
591

592 **Bonser, R. H. C. and Rayner, J. M. V.** (1996). Measuring leg thrust forces in the common
593 starling. *Journal of Experimental Biology* **199**, 435-439.
594

595 **Clark, J. and Alexander, R. M.** (1975). Mechanics of running by quail (*Coturnix*). *Journal*
596 *of Zoology* **176**, 87-113.
597

598 **Crandell, K. E. and Tobalske, B. W.** (2011). Aerodynamics of tip-reversal upstroke in a
599 revolving pigeon wing. *Journal of Experimental Biology* **214**, 1867-1873.
600

601 **Dabiri, J. O.** (2005). On the estimation of swimming and flying forces from wake
602 measurements. *Journal of Experimental Biology* **208**, 3519-3532.
603

604 **Dial, K. P.** (2003). Wing-assisted incline running and the evolution of flight. *Science* **299**,
605 402-404.
606

607 **Dial, K. P. and Biewener, A. A.** (1993a). Pectoralis-muscle force and power output during
608 different modes of flight in Pigeons (Columbia livia). *Journal of Experimental Biology* **176**,
609 31-54.
610

611 **Dial, K. P. and Biewener, A. A.** (1993b). Pectoralis muscle force and power output during
612 different modes of flight in Pigeons (Columbia livia). *Journal of Experimental Biology* **176**,
613 31-54.
614

615 **Dial, K. P., Jackson, B. E. and Segre, P.** (2008). A fundamental avian wing-stroke provides
616 a new perspective on the evolution of flight. *Nature (London)* **451**, 985-989.
617

618 **Dickinson, M. H., Lehmann, F. O. and Sane, S. P.** (1999). Wing rotation and the
619 aerodynamic basis of insect flight. *Science* **284**, 1954-1960.
620

621 **Dickinson, M. H., Farley, C. T., Full, R. J., Koehl, M. A. R., Kram, R. and Lehman, S.**
622 (2000). How animals move: An integrative view. *Science* **288**, 100-106.
623

624 **Doligalski, T. L., Smith, C. R. and Walker, J. D. A.** (1994). Vortex interactions with walls.
625 *Annual Review of Fluid Mechanics* **26**, 573-616.
626

Earls, K. D. (2000). Kinematics and mechanics of ground take-off in the starling *Sturnis Sturnus* vulgaris and the quail *Coturnix coturnix*. *Journal of Experimental Biology* **203**, 725-739.

Ellington, C. P. (1984). The aerodynamics of hovering insect flight .4. Aerodynamic mechanisms. *Philosophical Transactions of the Royal Society of London Series B-Biological Sciences* **305**, 79-&.

Garner, J. P., Taylor, G. K. and Thomas, A. L. R. (1999). On the origins of birds: the sequence of character acquisition in the evolution of avian flight. *Proceedings of the Royal Society of London Series B Biological Sciences* **266**, 1259-1266.

Gatesy, S. M. and Dial, K. P. (1993). Tail muscle-activity patterns in walking and flying pigeons (*Columbia livia*). *Journal of Experimental Biology* **176**, 55-76.

Gatesy, S. M. and Dial, K. P. (1996). Locomotor modules and the evolution of avian flight. *Evolution* **50**, 331-340.

Han, C. and Cho, J. (2005). Unsteady trailing vortex evolution behind a wing in ground effect. *Journal of Aircraft* **42**, 429-434.

Hartley, R. and Sturm, P. (1997). Triangulation. *Comput Vis Image Underst* **68**, 146–157.

Heppner, F. H. and Anderson, J. G. T. (1985). Leg thrust important in flight take-off in pigeon. *Journal of Experimental Biology* **114**, 285-288.

Jackson, B. E. and Dial, K. P. (2011). Scaling of mechanical power output during burst escape flight in the Corvidae. *Journal of Experimental Biology* **214**, 452-461.

Norberg, R. A. and Norberg, U. M. (1971). Take-off and landing and flight speed during fishing flights of *Gavia stellata*. *Ornis Scandinavica* **2**, 55-67.

Ostrom, J. H. (1974). Archaeopteryx and the origin of flight. *Quarterly Rev. Biol.* **49**, 27-47.

Padian, K. (1987). A comparative phylogenetic and functional approach to the origin of vertebrate flight. Cambridge: Cambridge University Press.

Provini, P., Goupil, P., Hugel, V. and Abourachid, A. (2012). Walking, paddling, waddling: 3D kinematics of Anatidae locomotion (*Callonetta leucophrys*). *Journal of Experimental Zoology* **317**, 275-282.

R Development Core Team. (2010). R: A Language and Environment for Statistical Computing. *R Foundation for Statistical Computing*.

Ros, I. G., Bassman, L. C., Badger, M. A., Pierson, A. N. and Biewener, A. A. (2011). Pigeons steer like helicopters and generate down- and upstroke lift during low speed turns. *Proceedings of the National Academy of Sciences of the United States of America* **108**, 19990-19995.

Rüppell, G. (1975). Bird flight. *Bird flight.*, 1-191.

Sane, S. P. (2003). The aerodynamics of insect flight. *Journal of Experimental Biology* **206**, 4191-4208.

Simpson, S. F. (1983). The flight mechanism of the pigeon *Columbia livia* during take-off. *Journal of Zoology* **200**, 435-443.

Spedding, G. R. (1993). On the significance of unsteady effects in the aerodynamic performance of flying animals. *Contemporary Mathematics* **141**, 401–419.

Spedding, G. R., Rosen, M. and Hedenstrom, A. (2003). A family of vortex wakes generated by a thrush nightingale in free flight in a wind tunnel over its entire natural range of flight speeds. *Journal of Experimental Biology* **206**, 2313-2344.

Tobalske, B. W. (2007). Biomechanics of bird flight. *Journal of Experimental Biology* **210**, 3135-3146.

Tobalske, B. W. and Dial, K. P. (2000). Effects of body size on take-off flight performance in the Phasianidae (Aves). *Journal of Experimental Biology* **203**, 3319-3332.

Tobalske, B. W. and Dial, K. P. (2007). Aerodynamics of wing-assisted incline running in birds. *Journal of Experimental Biology* **210**, 1742-1751.

Tobalske, B. W. and Biewener, A. A. (2008). Contractile properties of the pigeon supracoracoideus during different modes of flight. *Journal of Experimental Biology* **211**, 170-179.

Tobalske, B. W., Peacock, W. L. and Dial, K. P. (1999). Kinematics of flap-bounding flight in the zebra finch over a wide range of speeds. *Journal of Experimental Biology* **202**, 1725-1739.

Tobalske, B. W., Hedrick, T. L. and Biewener, A. A. (2003). Wing kinematics of avian flight across speeds. *Journal of Avian Biology* **34**, 177-184.

Tobalske, B. W., Altshuler, D. L. and Powers, D. R. (2004). Take-off mechanics in hummingbirds (Trochilidae). *Journal of Experimental Biology* **207**, 1345-1352.

Tobalske, B. W., Altshuler, D. L., Powers, D. R. (2004). Take-off mechanics in hummingbirds (Trochilidae). *Journal of Experimental Biology* **207**, 1345-1352.

Vogel, S. (1994). Life in moving fluids: the physical biology of flow,. Princeon, New Jersey.

Warrick, D. R., Tobalske, B. W. and Powers, D. R. (2005). Aerodynamics of the hovering hummingbird. *Nature* **435**, 1094-1097.

Table

Table 1: Morphometric parameters of zebra finch (*Taeniopygia guttata*) and diamond dove (*Geopelia cuneata*)

Species	Wing Length (cm)	Body Width (cm)	Wing Area (cm^2)	Wing Chord (cm)	Aspect Ratio	Tarsometatarsus Length (cm)
Zebra Finch	7.5 ± 0.4	2.4 ± 0.2	27.2 ± 2.3	4.1 ± 0.2	4.2 ± 0.04	1.6 ± 0.03
Diamond Dove	12.0 ± 0.4	2.8 ± 0.2	56.8 ± 4.8	5.5 ± 0.1	4.9 ± 0.05	1.7 ± 0.1

Table 2: Aerodynamic parameters for the first three wingbeats after *LO* in zebra finch (*Taeniopygia guttata*) (A) and diamond dove (*Geopelia cuneata*) (B). Diamond dove data for wingbeat three come from another experiment with the same methods but where birds were using level flight instead of climbing flight.

A

	zebra finch (*Taeniopygia guttata*)		
	Wingbeat 1	Wingbeat 2	Wingbeat 3
	Mean ± s.d.	Mean ± s.d.	Mean ± s.d.
A (cm^2)	163.64±17.7	193.82±22.3	177.88±6.5
Γ, $m^2\ s^{-1}$ (+)	0.35±0.1	0.42±0.2	0.5±0.02
Γ, $m^2\ s^{-1}$ (-)	-0.36±0.1	-0.54±0.1	-0.47±0.1

S (mm)	0.01±0.001	0.01±0.001	0.01±0.001
V_{vort} (m.s^{-1})	0.59±0.13	0.68±0.2	0.79±0.05
t_o (ms)	44.94±5.7	39.73±4.4	39.0±3.8
Angle of induced velocity to horizontal (degrees)	63.57±6.7	60.19±11.8	54.6±4.9
Magnitude of induced velocity (m.s^{-1})	3.9±1.9	5.1±2.3	5.1±1.6
V_{wtip} (m.s^{-1})	6.0±1.5	9.3±0.4	9.8±0.5
D_{wake} (m)	-	0.15±0.01	0.16 + 0.01
J_K	0.32±0.10	0.20±0.02	0.20±0.03
J_{PIV}	-	0.37±0.04	0.44±0.03

B

	diamond dove (*Geopelia cuneata*)		
	Wingbeat 1	Wingbeat 2	Wingbeat 3 *
	Mean ± s.d.	Mean ± s.d.	Mean ± s.d.
A (cm²)	461.34±40.9	462.66±33.4	399.2±40.4
Γ, m² s^{-1} (+)	0.58±0.2	0.71±0.1	0.46±0.1
Γ, m² s^{-1} (-)	-0.76±0.3	-0.79±0.1	0.57±0.1
S (mm)	0.01±0.001	0.01±0.001	0.01±0.001
V_{vort} (m s^{-1})	0.87±0.14	1.22±0.05	1.22±0.05
t_o (ms)	64.0±6.4	65.18±5.2	67.3±2.3
Angle of induced velocity to horizontal (degrees)	54.92±10.1	69.59±6.1	70.6±10.1
Magnitude of induced velocity (m.s^{-1})	4.37±1.3	5.22±1.3	4.0±0.8
V_{wtip} (m.s^{-1})	9.1±1.7	11.4±0.6	12.6±0.6
D_{wake} (m)	-	0.25±0	0.20±0.01
J_K	0.20±0.05	0.17±0.01	0.19±0.02
J_{PIV}	-	0.24±0.01	0.30±0.02

Figures

Fig. 1) A and C, velocity and B and D, acceleration, calculated from the displacement of the geometric center of the animal during take-off in zebra finch (*Taeniopygia guttata*), A and B and diamond dove (*Geopelia cuneata*), C and D. N=7 birds in zebra finch and N=3 in diamond dove with 5 trials within each bird. Envelopes illustrate the variability, defined as the maximum-minimum range across all trials. E) Sketch of the upstroke/downstroke succession during take-off.

In orange the horizontal component, in green the vertical component, in blue, the resultant (V_{RK}) and ($\dot{V}_{RK}$)

USDS: upstroke/downstroke transition; DSUS: downstroke/upstroke transition; LO: lift-off, FW: first use of the wings.

Fig. 2) Resultant acceleration ($\dot{V}_{RK}$) and resultant velocity (V_{RK}), calculated from the kinematic data (in blue) and from the force measurements ($\dot{V}_{RFP}$ and V_{RFP}, in pink) in zebra finch (*Taeniopygia guttata*) (A) and diamond dove (*Geopelia cuneata*) (B).

Fig. 3) Particle image velocimetry. A and C, velocity vectors, expressed relative to average velocity, and with background vorticity (ω), B and D, Streamlines associated with the vector field. Broken lines indicate regions sampled for ω (red=starting vortex, blue=ending vortex) in zebra finch (*Taeniopygia guttata*) (A and B) and diamond dove (*Geopelia cuneata*) (C and D). Grey circle highlights the location of the take-off perch.

Fig. 4) Category plot of the acceleration produced during the first three wingbeats in zebra finch (*Taeniopygia guttata*) (A) and in diamond dove (*Geopelia cuneata*) (B). In blue, resultant acceleration calculated from kinematic data ($\dot{V}_{RK}$) for 5 trials in N=7 zebra finches and N=3 diamond doves during the first upstroke and during each wingbeat. In pink, resultant acceleration calculated from the force data ($\dot{V}_{RFP}$) for 5 trials in N=7 zebra finches and N=3 diamond doves during the first upstroke and first wingbeat. In orange, resultant acceleration calculated from PIV data ($\dot{V}_{PIV}$) with N=4 zebra finches and 37 wingbeats and N=3 diamond doves and 42 wingbeats.

Electronic supplementary material

Supplemental Figure S1: Drawing of a zebra finch (*Taeniopygia guttata*) with the position of the digitized landmarks and the edge of the animal used to calculate the position of the

770 geometric center. The position of the center of mass estimated using the multiple suspension
771 method is represented by a circle.
772
773 Supplementary Figure S2: A) Vertical trajectory of the center of mass over time in zebra finch
774 (*Taeniopygia guttata*) (purple) and diamond dove (*Geopelia cuneata*) (pink) and B) Body
775 orientation in zebra finch (purple) and diamond dove (pink). Time zero is at lift-off.

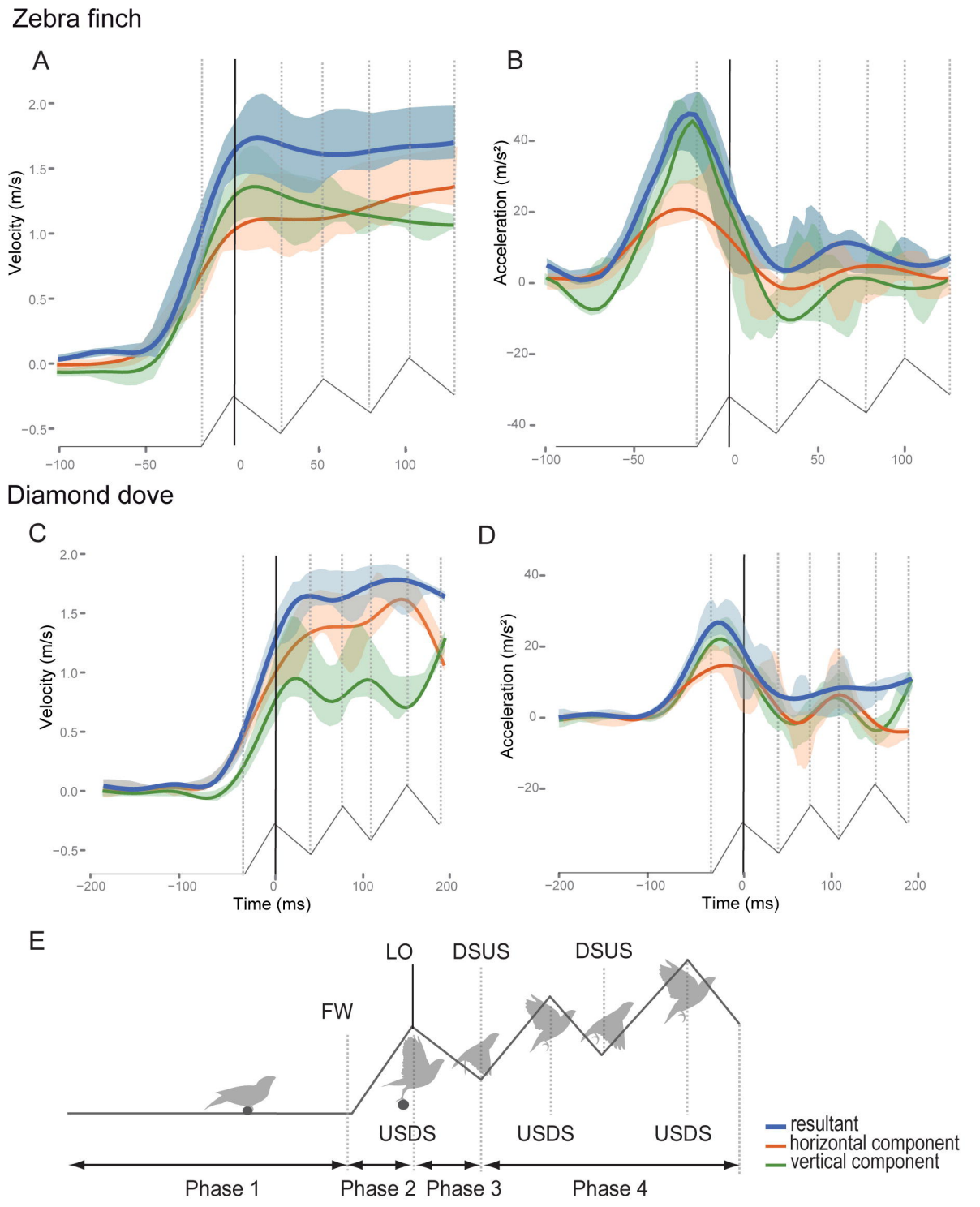
Zebra finch
A
B
Velocity (m/s)
Acceleration (m/s²)
Diamond dove
C
D
Time (ms)
E
LO
DSUS
DSUS
FW
USDS
USDS
USDS
Phase 1
Phase 2
Phase 3
Phase 4
resultant
horizontal component
vertical component

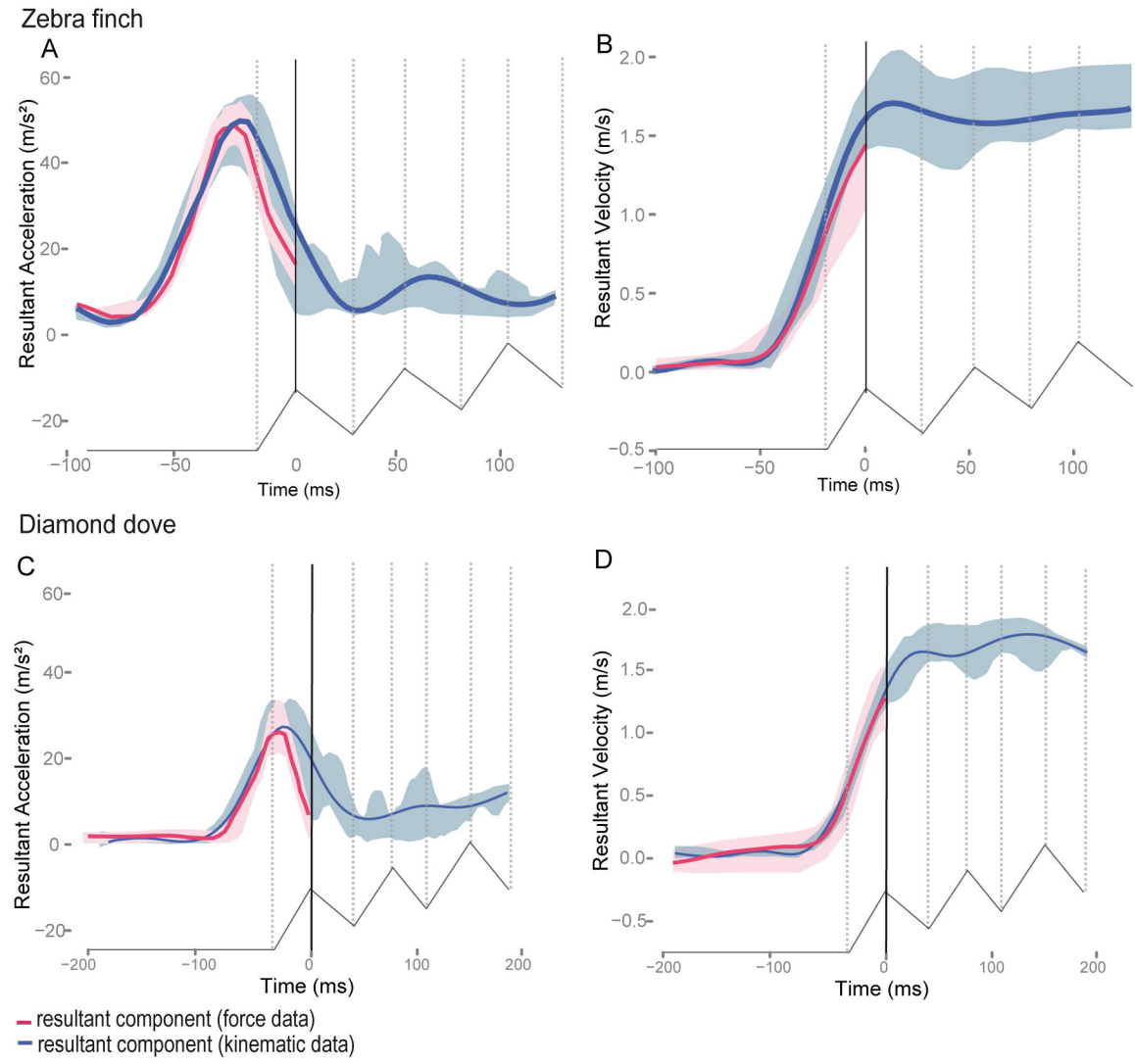
Zebra finch
A
B
Resultant Acceleration (m/s²)
Resultant Velocity (m/s)
Time (ms)
Diamond dove
C
D
resultant component (force data)
resultant component (kinematic data)

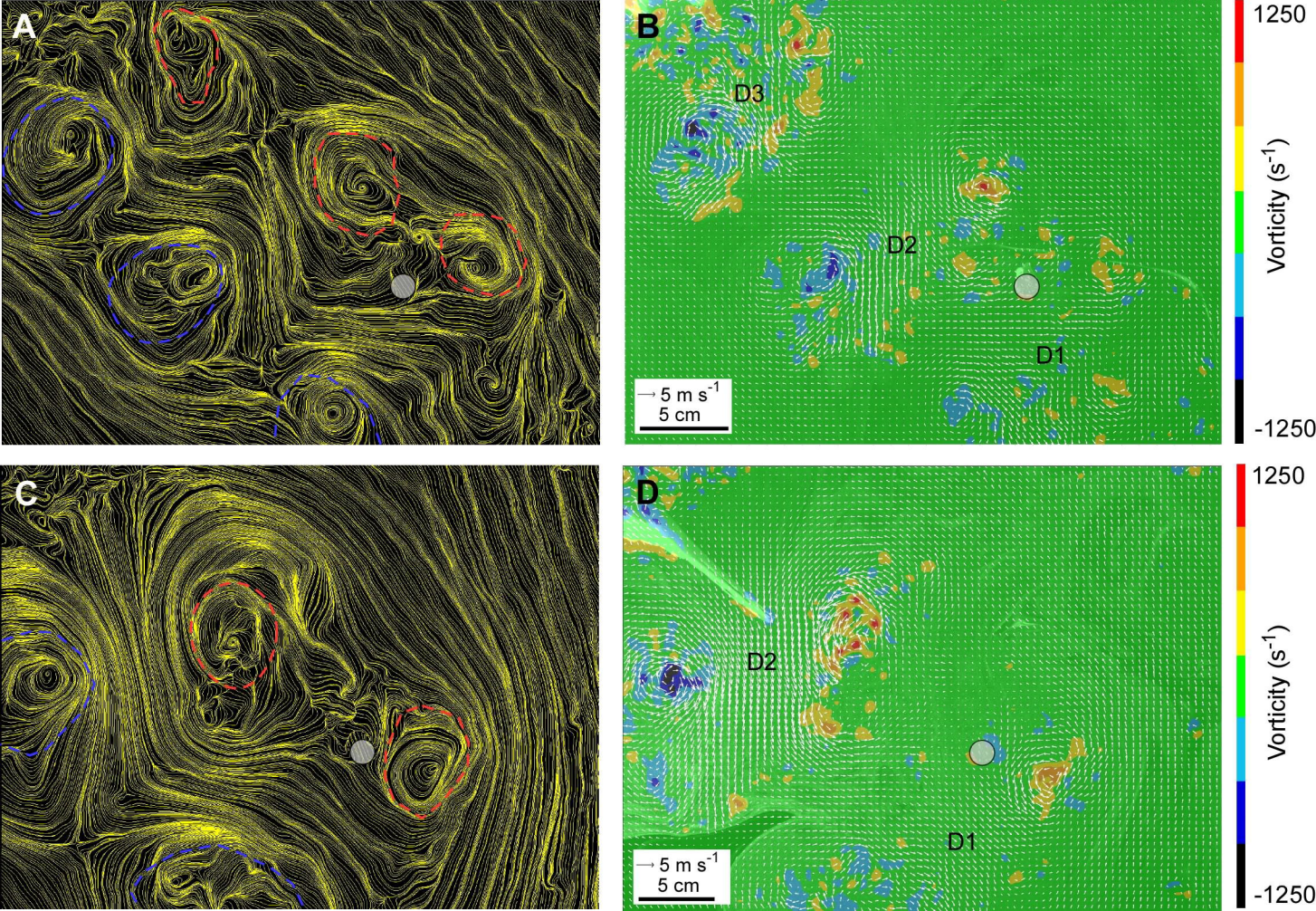
A
B
D3
D2
D1
5 m s-1
5 cm
1250
Vorticity (s-1)
-1250
C
D
D2
D1
5 m s-1
5 cm
1250
Vorticity (s-1)
-1250

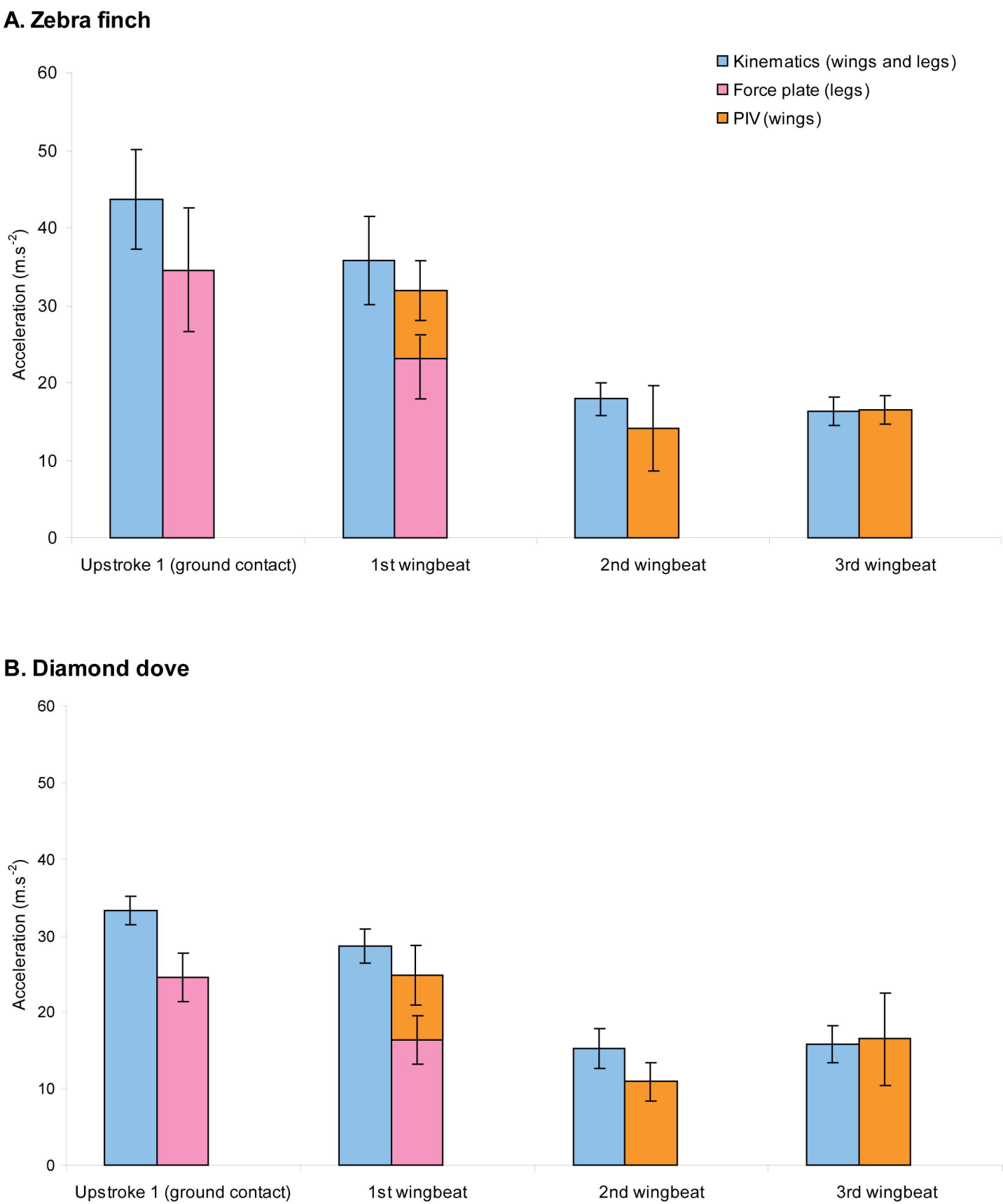
A. Zebra finch
Kinematics (wings and legs)
Force plate (legs)
PIV (wings)
Acceleration (m.s-2)
60
50
40
30
20
10
0
Upstroke 1 (ground contact)
1st wingbeat
2nd wingbeat
3rd wingbeat
B. Diamond dove
Acceleration (m.s-2)
60
50
40
30
20
10
0
Upstroke 1 (ground contact)
1st wingbeat
2nd wingbeat
3rd wingbeat